elevated fields, consistent with the evolution of the $M(T)$ peak as a function of field [section C of (17)].

Figure 4 describes a possible scenario for the two stages of transitions. Below T_{AF}, the Néel order develops. We speculate that the growth of the Néel order parameter m_{AF} is arrested as the temperature is lowered past T_{hyb}, due to the onset of the nuclear spin order. A diminished m_{AF} would place the electronic phase in the regime close to the QCP that underlies the pure electronic system in the absence of any hyperfine coupling. This quantum criticality effectively induced by the nuclear spin order at zero magnetic field would naturally lead to the development of a superconducting state [section I of (17)]. As inferred from the experimental results (Fig. 1C), fluctuations of the A phase are already set in near T_B and lead to a substantial reduction of the staggered magnetization and the emergence of superconducting fluctuations well above the A-phase ordering temperature [section I of (17)].

The large initial slope of the superconducting upper critical field $B_{c2}(T)$ at $T_c \simeq 25$ T/K, extracted from both shielding (Fig. 3, inset) and Meissner measurements (fig. S3C), corresponds to an effective charge-carrier mass of several hundred m_e (where m_e is the rest mass of the electron), which implies that the superconducting state is associated with the Yb-derived 4f electrons (heavy-electron superconductivity). Extrapolating the positions of the low-temperature fc $M(T)$ peak to zero temperature, the critical field of the A phase $B_A = B(T_A \rightarrow 0)$ is found to be 30 to 60 mT, which corresponds to $g_{eff} = k_B T_A(B = 0)/\mu_B B_A = 0.03$ to 0.06 (where k_B is the Boltzmann constant and μ_B is the Bohr magneton). This value of g_{eff} is much smaller than the in-plane electronic g-factor 3.5 (24) but is a factor of 20 to 40 larger than in case of a purely nuclear spin ordering transition. We can understand this g_{eff} if the ordered moment is a hybrid of the electronic and nuclear spins with, at most, 2% of the ordered moments being associated with the 4f electron–derived spins.

The very large entropy near $T_A \geq 2$ mK is one of the most pronounced features in our observation. An alternative possibility for this entropy is the involvement of a "nuclear Kondo effect"—that is, the formation of a singlet state between the nuclear and conduction electron spins. The resulting superheavy fermions may be assumed to form Cooper pairs and cause a superconducting transition at $T_c \approx 2$ mK that would be probed by the magnetic and specific-heat measurements. Though our estimates of the nuclear Kondo temperature and the quasi-particle effective mass reveal discrepancies with this picture [section E of (17)], further theoretical and experimental work is needed to investigate the possible role of the nuclear Kondo effect in generating superconductivity in $YbRh_2Si_2$.

It is likely that the coupling of electronic and nuclear spin orders, as well as the concomitant emergence of new physics, is not exclusive to $YbRh_2Si_2$ [section H of (17)]. Systematic studies of other heavy-electron antiferromagnets at ultralow temperatures are needed to find out whether a hybrid electronic-nuclear order is a more general phenomenon. In addition, a comparative study would be highly welcome to evaluate whether superconductivity is truly absent in isotopically enriched $YbRh_2Si_2$ without Yb-derived nuclear spins, similar to the compound studied in (25).

Our ultralow-temperature measurements on the unconventional quantum critical material $YbRh_2Si_2$ reveal heavy-electron superconductivity below $T_c = 2$ mK. This observation strongly supports the notion that superconductivity near an AF instability is a robust phenomenon.

REFERENCES AND NOTES

1. P. A. Lee, N. Nagaosa, X.-G. Wen, *Rev. Mod. Phys.* **78**, 17–85 (2006).
2. H. Löhneysen, A. Rosch, M. Vojta, P. Wölfle, *Rev. Mod. Phys.* **79**, 1015–1075 (2007).
3. P. Gegenwart, Q. Si, F. Steglich, *Nat. Phys.* **4**, 186–197 (2008).
4. N. D. Mathur *et al.*, *Nature* **394**, 39–43 (1998).
5. O. Stockert *et al.*, *Nat. Phys.* **7**, 119–124 (2011).
6. J. Custers *et al.*, *Nature* **424**, 524–527 (2003).
7. H. Shishido, R. Settai, H. Harima, Y. Ōnuki, *J. Phys. Soc. Jpn.* **74**, 1103–1106 (2005).
8. T. Park *et al.*, *Nature* **440**, 65–68 (2006).
9. G. Knebel, D. Aoki, J.-P. Brison, J. Flouquet, *J. Phys. Soc. Jpn.* **77**, 114704 (2008).
10. H. Löhneysen *et al.*, *Phys. Rev. Lett.* **72**, 3262–3265 (1994).
11. A. Schröder *et al.*, *Nature* **407**, 351–355 (2000).
12. S. Paschen *et al.*, *Nature* **432**, 881–885 (2004).
13. S. Friedemann *et al.*, *Proc. Natl. Acad. Sci. U.S.A.* **107**, 14547–14551 (2010).
14. Q. Si, S. Rabello, K. Ingersent, J.-L. Smith, *Nature* **413**, 804–808 (2001).
15. P. Coleman, C. Pépin, Q. Si, R. Ramazashvili, *J. Phys. Condens. Matter* **13**, R723–R738 (2001).
16. T. Senthil, M. Vojta, S. Sachdev, *Phys. Rev. B* **69**, 035111 (2004).
17. Supplementary materials are available on *Science* Online.
18. E. Schuberth, M. Tippmann, C. Krellner, F. Steglich, *Phys. Stat. Solidi B* **250**, 482–484 (2013).
19. F. Steglich *et al.*, *Phys. Rev. Lett.* **43**, 1892–1896 (1979).
20. A. Steppke *et al.*, *Phys. Stat. Solidi B* **247**, 737–739 (2010).
21. H. M. Rønnow *et al.*, *Science* **308**, 389–392 (2005).
22. K. Andres, E. Bucher, P. H. Schmidt, J. P. Maita, S. Darack, *Phys. Rev. B* **11**, 4364–4372 (1975).
23. L. Steinke *et al.*, *Phys. Rev. Lett.* **111**, 077202 (2013).
24. J. Sichelschmidt, V. A. Ivanshin, J. Ferstl, C. Geibel, F. Steglich, *Phys. Rev. Lett.* **91**, 156401 (2003).
25. G. Knebel *et al.*, *J. Phys. Soc. Jpn.* **75**, 114709 (2006).

ACKNOWLEDGMENTS

We thank K. Andres, P. Coleman, P. Gegenwart, S. Paschen, and S. Wirth for useful discussions. Part of the work at the Max Planck Institute for Chemical Physics of Solids was supported by the Deutsche Forschungsgemeinschaft Research Unit 960 "Quantum Phase Transitions." Q.S. was supported by NSF grant DMR-1309531 and Robert A. Welch Foundation grant C-1411. E.S., Q.S., and F.S. thank the Institute of Physics, Chinese Academy of Sciences, Beijing, for hospitality. Q.S. and F.S. acknowledge partial support from the NSF under grant 1066293 and the hospitality of the Aspen Center for Physics. We declare no competing financial interests.

SUPPLEMENTARY MATERIALS

www.sciencemag.org/content/351/6272/485/suppl/DC1
Materials and Methods
Supplementary Text
Figs. S1 to S9
References (26–65)

23 February 2015; accepted 16 December 2015
10.1126/science.aaa9733

GEOPHYSICS

Periodic slow slip triggers megathrust zone earthquakes in northeastern Japan

Naoki Uchida,[1]* Takeshi Iinuma,[2]† Robert M. Nadeau,[3] Roland Bürgmann,[4] Ryota Hino[1]

Both aseismic and seismic slip accommodate relative motion across partially coupled plate-boundary faults. In northeastern Japan, aseismic slip occurs in the form of decelerating afterslip after large interplate earthquakes and as relatively steady slip on uncoupled areas of the subduction thrust. Here we report on a previously unrecognized quasi-periodic slow-slip behavior that is widespread in the megathrust zone. The repeat intervals of the slow slip range from 1 to 6 years and often coincide with or precede clusters of large [magnitude (M) ≥ 5] earthquakes, including the 2011 M 9 Tohoku-oki earthquake. These results suggest that inherently periodic slow-slip events result in periodic stress perturbations and modulate the occurrence time of larger earthquakes. The periodicity in the slow-slip rate has the potential to help refine time-dependent earthquake forecasts.

Slow (or aseismic) slip is a process by which faults displace rocks like earthquakes do, but much more slowly and without generating seismic waves (1, 2). Slow fault-slip events increase stress in adjacent areas and may trigger damaging earthquakes (3). Foreshocks are sometimes related to precursory slow slip (4–6), and some slow-slip events revealed by geodetic measurements are accompanied by seismicity rate changes (7). However, the relationship between large earthquakes and aseismic slip is not well understood because of the poor detectability of small slow-slip events with geodetic measurements and the rare occurrence of large earthquakes. We understand that repeating earthquakes involve the rupture of small asperities in the fault zone as seismic slips keep up with aseismic fault creep (slow slip) on the surrounding surface (*8*) (Fig. 1). Repeating earthquakes provide a remote measure of both localized seismic slip and the surrounding rate of aseismic slip on a fault that greatly improves the spatiotemporal resolution of slow slip (*4*, *9*, *10*). In this study, we refer to repeating earthquakes as "repeaters" and invoke them as a form of subsurface creep meter (Fig. 1). Here we consider repeater time series and global positioning system (GPS) measurements from the northeastern (NE) Japan subduction zone to detect small temporal changes in the slow-slip rate. Major earthquakes, including the great 2011 Tohoku-oki earthquake [magnitude (*M*) 9.0], also occur on the offshore plate interface between the subducting Pacific and continental plates (Fig. 2A) (*1*, *4*, *11*–*13*).

We examined the seismic moments and recurrence intervals of 6126 repeaters belonging to 1515 separate sequences to detect interplate slip-rate fluctuations for a period of up to 28 years (*14*) (table S1). In the offshore and near-shore Sanriku areas (Fig. 2), the slow-slip rates are estimated from 162 and 91 repeater sequences, respectively, using a 0.5-year moving time window, with the average rates plotted at the center of each time window (*14*) (Fig. 1). The variations in slip rate ranged from 0 to 290% of the long-term interplate slip rate (*15*) (7.4 ± 0.2 cm/year) and showed strong periodicity. The amplitude of the inferred slip rate depends on the length of the analysis window and the scaling relationship used to estimate the slip amount, but the periodicity is not affected by these conditions (*14*).

We estimated the dominant periods of slow slip, based on spectral analysis, to be 3.0 ± 0.1 SD years for the offshore Sanriku area (Fig. 2B and fig. S4I) and 2.7 ± 0.6 years for near-shore Sanriku area (Fig. 2C and figs. S4J and S5) (*14*). Two large slip-velocity peaks in 1990 and 1992 could bias the spectral estimate of period in the offshore Sanriku area (Fig. 2B), but analysis excluding data before 1992 also shows a similar dominant period (fig. S4I). We compared the timing of $M \geq 5$ events (Fig. 2, B and C) to the regional slip rate. The magnitude threshold was chosen to ensure a complete catalog for our analysis period and a big enough sample of larger events. Clustering of $M \geq 5$ earthquakes in the high slip-rate periods is evident, especially in the offshore area (Fig. 2B). We fitted simple sinusoidal curves to the slip-rate changes to define the phase of the periodicity, finding that 6.2 and 3.3 times as many 1984–2011 $M \geq 5$ earthquakes occurred during the positive period of the best-fit sinusoids for the offshore and near-shore Sanriku areas, respectively (Fig. 2, B and C; fig. S6, C and D; and table S2). We calculated the excess number of $M \geq 5$ earthquakes for a range of periods and found that they decay away ±0.15 years from the best-fit periods we established from the repeater data (fig. S6). We showed a concentration of $M \geq 5$ earthquakes near the inferred slip-rate peak (fig. S7), using histograms of earthquake occurrence with respect to phase of the best-fit sinusoids. We found a similar correlation between periodic slow-slip rates and large earthquakes for most of the eight offshore areas where we documented the distribution of repeaters and earthquakes (fig. S2 and table S2).

When we applied declustering to the earthquake catalog with a range of declustering parameters, the number of excess earthquakes in the positive period of the best-fit sinusoids decreased (tables S3 and S4). Although the excess ratios for the offshore Sanriku area range from 2.0 to 2.8, those for the near-shore Sanriku area are systematically reduced to 1.2, suggesting that clusters associated with large earthquakes influence the result.

A possible explanation for the correlated periodicity (Fig. 2 and fig. S7) is that periodically occurring $M \geq 5$ events and their afterslip trigger the smaller repeaters. However, close inspection of the repeater activity and inferred slip-rate changes for the major slip pulses in 1989–1990 and 1992 in the offshore Sanriku area (Fig. 3A) shows that the repeater-inferred slow slip begins accelerating a few days before the mainshocks associated with the slip pulses (*16*). The precursory repeater activity is a common feature before $M \geq 5$, $M \geq 6$, and $M \geq 7$ earthquakes (mainshocks) in the offshore Sanriku area and most of the other study areas (figs. S8 and S9). The precursory repeater accelerations concentrate close to mainshock epicenters (figs. S10 and S11), suggesting

[1]Graduate School of Science and International Research Institute of Disaster Science, Tohoku University, 6-6, Aramaki-aza-aoba, Aoba-ku, Sendai 980-8578, Japan. [2]International Research Institute of Disaster Science, Tohoku University, 468-1, Aramaki-aza-aoba, Aoba-ku, Sendai 980-0845, Japan. [3]Berkeley Seismological Laboratory and Berkeley Institute for Data Science, University of California, Berkeley, 211 McCone Hall, Berkeley, CA 94720-4767, USA. [4]Berkeley Seismological Laboratory and Department of Earth and Planetary Science, University of California, Berkeley, 389 McCone Hall, Berkeley, CA 94720-4767, USA.
***Corresponding author. E-mail: naoki.uchida.b6@tohoku.ac.jp**
†Present address: Japan Agency for Marine-Earth Science and Technology, Yokohama, 236-0001, Japan.

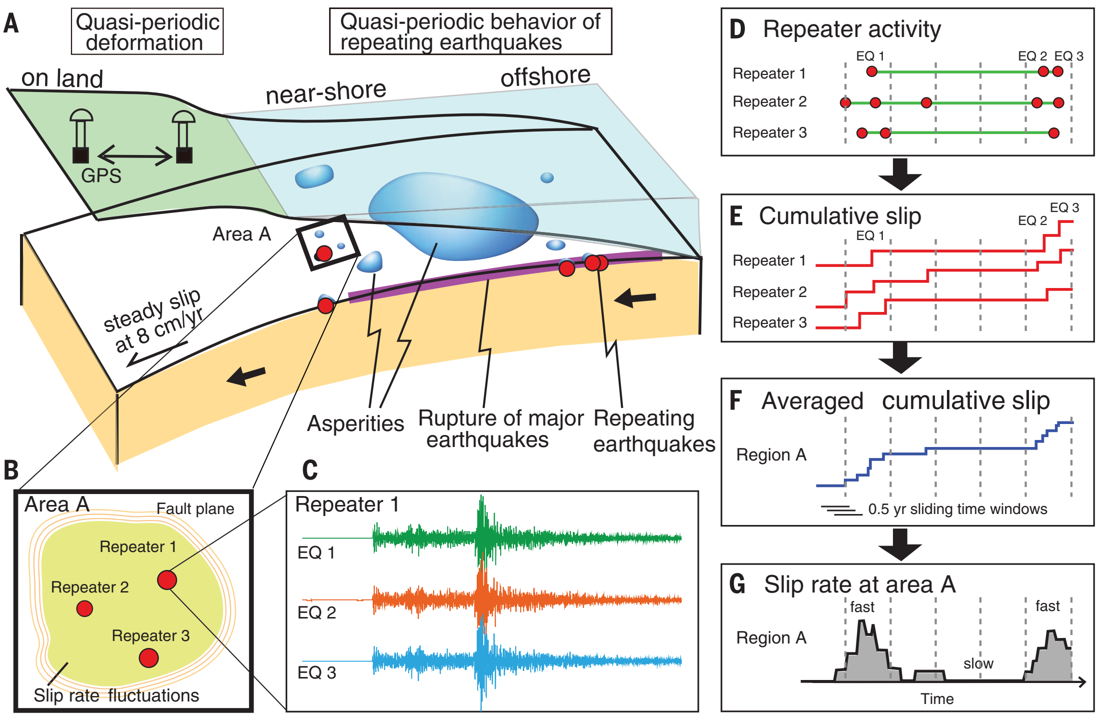

Fig. 1. Using repeaters to track slow plate-boundary slip. Schematic figure showing the tectonic setting (**A**), the activity of repeaters on the plate boundary (**B** and **C**), and steps to estimate the slip-rate time series from repeater data (**D** to **G**) (*14*). There are variably sized seismic patches on the plate boundary surrounded by aseismic slip areas (A). The small repeaters (C) represent repeated rupture of small patches that catch up with the creep in the surrounding areas (B). By calculating the slip of each earthquake, we obtain cumulative slip for each repeater sequence [(D) and (E)]. We average slip in each area (F) and obtain the temporal change of slip rate from the gradient of the averaged cumulative curve (G).

close interaction with the preceding repeater activity. Mainshocks are also generally followed by accelerated repeater activity (figs. S8 and S9), indicating rapid afterslip.

Marsan *et al.* (*17*) suggest occurrences of many slow-slip episodes in this subduction zone by discriminating normal from "abnormal" seismicity affected by transient loading. The activity of small repeaters indicates the involvement of spontaneous slow-slip events as the underlying aseismic loading process driving these episodic deformation transients. Observations from ocean-bottom pressure sensors of slow slip preceding *M* 6.1 and *M* 7.3 earthquakes occurring ~100 km south of this area in 2008 and 2011 (green stars in Fig. 2A) (*18*), respectively, are also consistent with this interpretation.

We tested the hypothesis of an ~3-year periodic slow slip promoting $M \geq 5$ earthquakes in the offshore Sanriku area by extrapolating the sinusoidal curve from the 1984 to 2011 slip-rate data back to 1930 (red curve in Fig. 3C). The positive phase of the sinusoidal curve (expected high–slip-rate periods) correlates with higher rates of $M \geq 5$ earthquakes back to around 1945 (Fig. 3C). The number of $M \geq 5$ earthquakes occurring during positive sinusoid amplitudes for the period 1956–1983 is about twice as high as the number of events occurring during negative sinusoid amplitudes (dashed curve in fig. S6C).

Our sinusoidal extrapolation of the slow slip assumes exact periodicity of the process, and slight shifts in the period result in large shifts in the timing of sinusoid peaks when extrapolating over many years. To address this, we examined the periodicity of the $M \geq 5$ declustered catalog using the Schuster spectrum (*19*). Our results show an ~3-year periodicity for the offshore Sanriku area (Fig. 3B) for all time spans considered, including the repeater analysis period. We do not find as strong a periodicity for the near-shore area (figs. S5A and S6D). Our

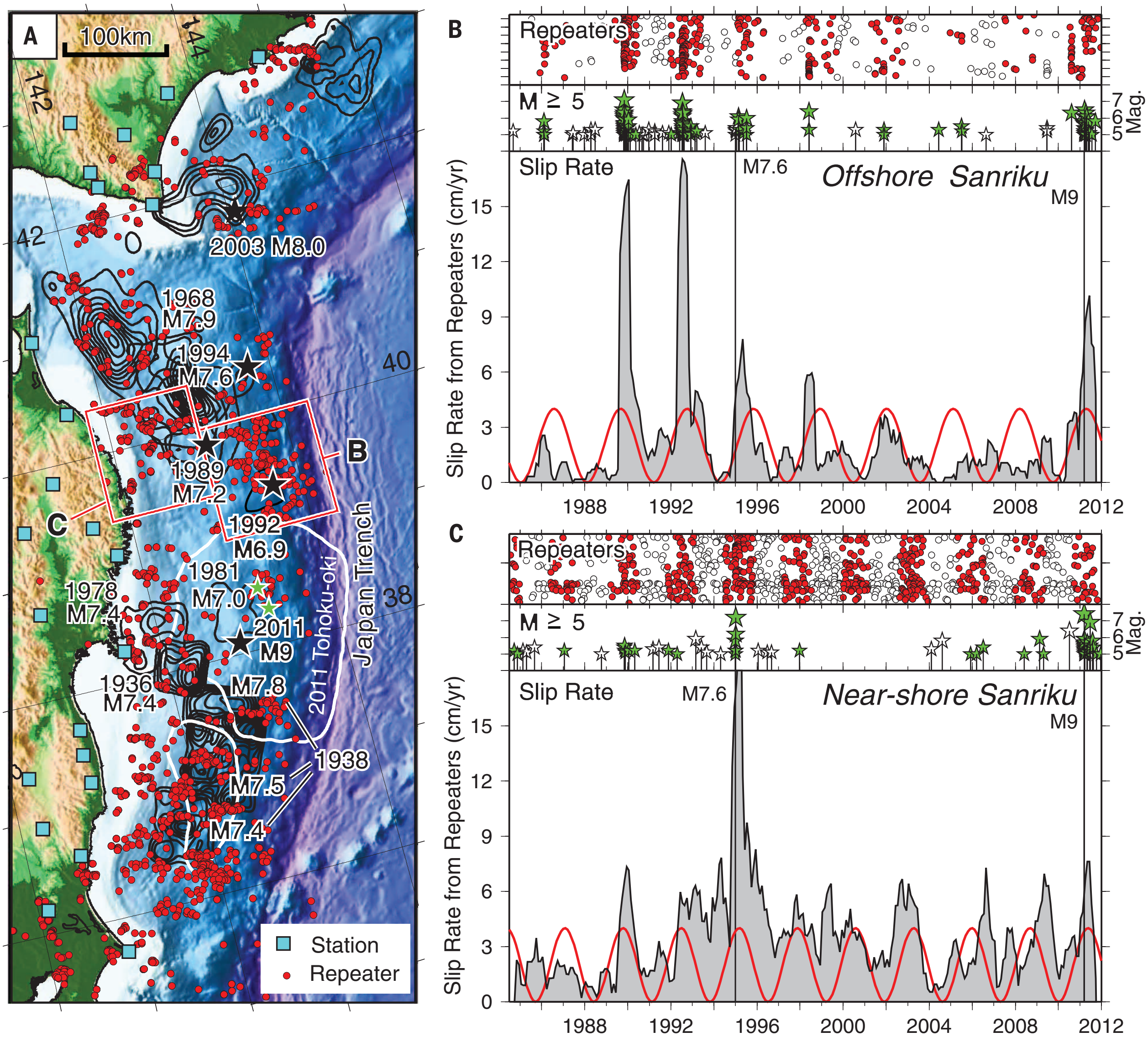

Fig. 2. Spatiotemporal distribution of repeaters and temporal variation of slow slip. (**A**) Distribution of repeater sequences (red circles) and slip areas of large earthquakes (black and white contours) (*11*–*13*, *29*, *30*). Cyan squares show seismic stations. Green stars show a *M* 6.1 earthquake in 2008 (north) and a *M* 7.3 earthquake in 2011 (south) that were preceded by slow slip (*18*). (**B** and **C**) Temporal distribution of repeaters near Sanriku aligned by latitude (top) (see fig. S1 for vertical enlargement), magnitude-time plot of $M \geq 5$ earthquakes (middle), and temporal change of slip rate inferred from repeaters (bottom) for offshore (B) and near-shore (C) areas off Sanriku shown in (A) (see fig. S3 for corresponding data for all other areas). Vertical lines show the times of the 1994 *M* 7.6 Sanriku-oki and the 2011 *M* 9 Tohoku-oki earthquakes. The number of $M \geq 5$ events in offshore and near-shore areas is 194 and 68, respectively. The red curves in (B) and (C) are best-fit sinusoidal functions fit to the slip-rate time series with 3.09- and 2.72-year periods, respectively. Repeaters and $M \geq 5$ events during the positive phase of the best-fitted sinusoid are shown by colored symbols, whereas those during the negative phase are shown by open symbols.

consideration of ~80 years of earthquakes offshore of Sanriku suggests that the periodicity of slow slip and associated larger earthquakes persists through time before the repeater analysis period.

Continuous GPS measurements across NE Japan provide complementary constraints on the time-variable coupling of the subduction thrust from the repeater data. The spatial gradient of observed displacement rates in the plate convergence direction reflects the strength of interplate locking and associated slip (*20*) (figs S12 and S13) (*14*), and its temporal variation may be a measure of the acceleration/deceleration of aseismic slip along the plate boundary. Although we infer that repeaters directly track slip on the subduction thrust, the on-land GPS data are only indirectly related to changing fault slip via elastic deformation. In order to stabilize the estimate of the time-dependent gradient of the displacement rate (the GPS gradient), we used a longer moving time window of 1 year. Periods of more negative GPS-gradient values, reflecting increased shortening, indicate times of stronger locking or lower slow-slip rates in the offshore area (fig. S12). The time series estimated from the observationally independent GPS gradient show similar fluctuations as those of the repeater slip rates (fig. S3).

We performed a moving spatial window analysis of the slip-rate spectrum to comprehensively examine the spatial distribution of the degree of periodicity and its dominant period along the NE Japan subduction zone. For each area, we determined the period of peak amplitude (short black vertical line in Fig. 3B) within the 1- to 9-year range and the degree of periodicity from the amplitude ratio of peak and average (red horizontal dashed line in Fig. 3B) amplitudes in the same period range. We used 0.4° (latitude) by 0.6° (longitude) spatial windows with 10 or more repeater sequences, showing widespread periodic behavior across the subduction zone (Fig. 4). The uncertainties of the estimated periodicities are generally on the order of 1 year (fig. S2B) (*14*). The dominant period has a heterogeneous distribution in both dip and strike directions (Fig. 4 and fig. S2A). Much of the subduction zone shows periods that range from 1 to 6 years and agrees with the periodicity of $M \geq 5$ earthquakes where strong slow-slip periodicity exists (fig. S2C). Around the slip areas of previous large earthquakes (*11*, *12*), including the 2011 Tohoku-oki earthquake (*13*), the aseismic slip rates are generally low and the periodicity is weak (light color in Fig. 4), with relatively long periods (>5 years). The relatively long period in the southern part of the coseismic slip area of the 2011 Tohoku earthquake (36.5° to 38°N) is consistent with a 5.9-year periodicity inferred from seismicity data for this area (*17*). The relatively weak periodicity near the large earthquakes may reflect the inhibition of periodic slip by strong interplate locking or indicate periods that are longer than the observation period.

The overall pattern of the offshore slip-rate periodicity from the repeater data correlates with the periods inferred from GPS gradients along profiles perpendicular to the margin (circles in Fig. 4 and fig. S13). A comprehensive evaluation of temporal slip-rate changes inferred from repeaters and GPS along the NE Japan subduction zone (figs. S2 to S4) shows correlations between the GPS gradients and near-shore repeater slip rates. The large variability in the correlations is probably due to the small-scale heterogeneities in periodic slow-slip behavior on the interplate fault in both along-dip and strike directions.

Periodic fault behavior may be driven by external forcing by tidal, atmospheric, and hydrologic cycles over a wide range of periods (*21*–*23*). However, we are unaware of forcing processes that recur at the most common periods we observe of 2 to 3 years (Fig. 4). Modeling

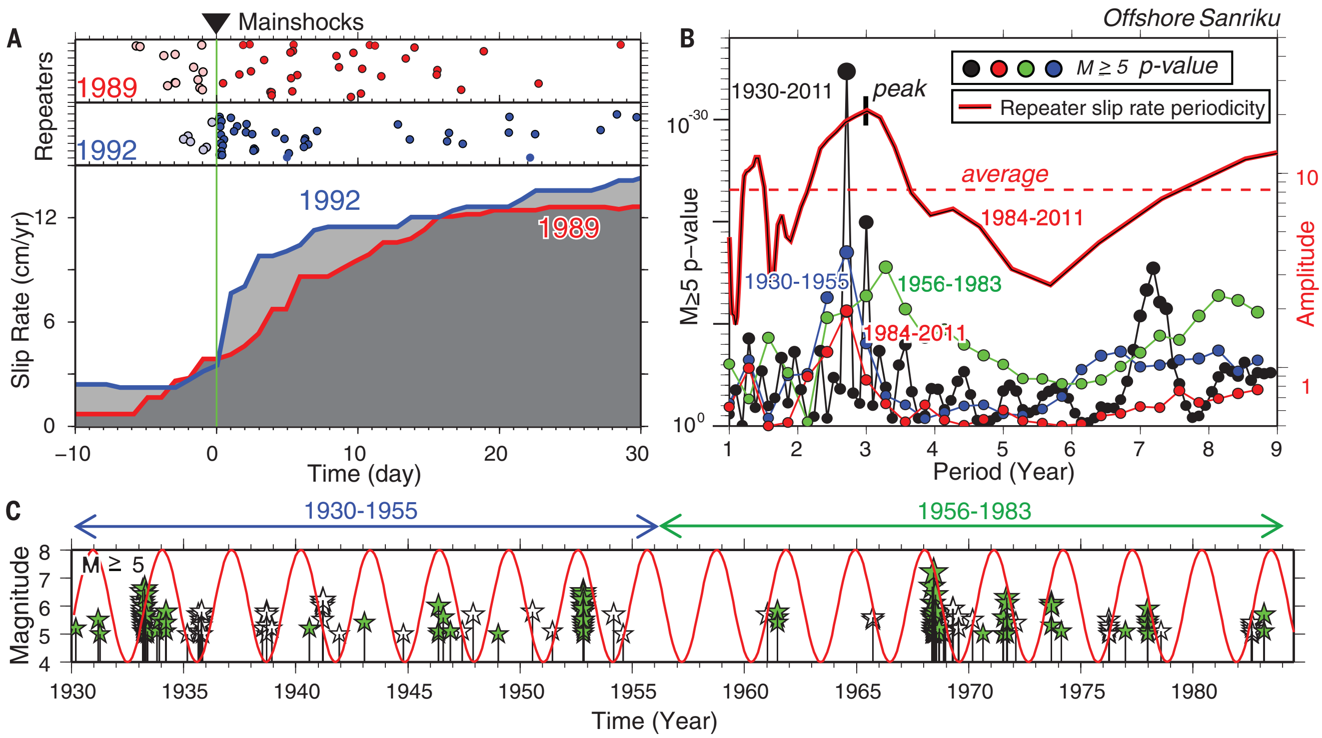

Fig. 3. Timing of repeaters, slow slip, and $M \geq 5$ earthquakes. (**A**) Times of the repeaters (top panels) and repeater-inferred slip rates (bottom panel) in the offshore Sanriku area (Fig. 2B) around the times of the 1989 *M* 7.2 (red) and 1992 *M* 6.9 (blue) mainshocks. Slip rates during 10 days before and 30 days after the mainshocks are plotted using a causal data window stepped every 1 day. Light and deep colors for the circles indicate repeaters before and after the mainshocks, respectively. (**B**) Amplitude spectrum of the slip rate for the offshore Sanriku area (red line; the original slip-rate time series is shown in Fig. 2B). The horizontal dashed red line shows the average of the amplitude in a 1- to 9-year period range. Black, red, green, and blue circles show Schuster spectra (*19*) for the $M \geq 5$ declustered earthquake catalogs for the time periods shown in the figure. The *P* values on the vertical axis give the probability of observing such a level of periodic variations in a catalog with a constant seismicity rate. (**C**) Magnitude-time plot of $M \geq 5$ earthquakes in the offshore Sanriku area before the repeater analysis period (i.e., 1930 to 1983). The red curve is the same sinusoidal function as in Fig. 2B, extrapolated from the fitting period. The green and white stars show events during times of positive and negative amplitude of the extrapolated sinusoid, respectively. Green and blue lines show the time period used in Fig. 3B. Plots similar to Fig. 3, B and C, but for the near-shore Sanriku area are shown in fig. S5, A and B, respectively.

studies suggest that slow-slip event periodicity may be governed by fault zone properties, including dilatancy, permeability, fluid pressure, and healing rates (*24*, *25*). Audet and Bürgmann (*26*) draw on the observed correlation of recurrence periods of deep slow-slip events in global subduction zones with seismic velocity variations to support a scenario of slow-slip event periodicity being governed by fault zone properties. The enduring nature of the periodic behavior we document suggests that fault zone constitutive properties could govern the recurrence of slow-slip events off northern Japan.

The 2011 Tohoku-oki earthquake occurred 0.7 years before the end of our analysis period. Slip rate peaks in the off-Sanriku areas before the 2011 Tohoku-oki earthquake, and the subsequent timing of the 2011 earthquake falls in the positive period of the sinusoidal slip-rate curve (Fig. 2, B and C), although the accelerations are not as obvious in the southern areas (fig. S3, E and F). Slow slip was detected in 2008 and 2011 from ocean-bottom pressure sensors (*18*) to the south of the off-Sanriku area. The slip episode appears to have triggered the largest foreshock (*M* 7.3) that occurred 2 days before the Tohoku-oki earthquake (*18*). Preseismic slow-slip migration toward the mainshock hypocenter occurred in February to March 2011 (*4*), but no significant preslip was detected on the megathrust fault immediately before the Tohoku-oki earthquake, from the analysis of seafloor vertical deformation data near the epicenter (*27*).

Large postseismic slip continues off Tohoku (*28*). If the inherent fault zone properties govern the periodicity of slow-slip transients, the periodicity may not change because of the Tohoku-oki earthquake. Previous examples support this scenario: The first slow-slip acceleration after the 1994 Sanriku-oki earthquake (*M* 7.6) that occurred just north of the Sanriku area (Fig. 2A) started somewhat earlier, but the period and phase did not change much for later slip accelerations in the offshore Sanriku area (Fig. 2B). In the case of the 2003 Tokachi-oki earthquake (*M* 8.0), the periodicity in the offshore area only became prominent after the earthquake (fig. S3C).

In most probabilistic earthquake forecasts based on recurrence intervals and time since the last event, a constant loading rate is implicitly assumed. The inherent periodicity of slow slip found in this study suggests that probabilistic forecasts of future earthquakes can be improved by explicitly considering cyclic loading-rate changes.

The real-time monitoring of slow slip may also help improve the estimation of time-dependent earthquake hazards (*29*).

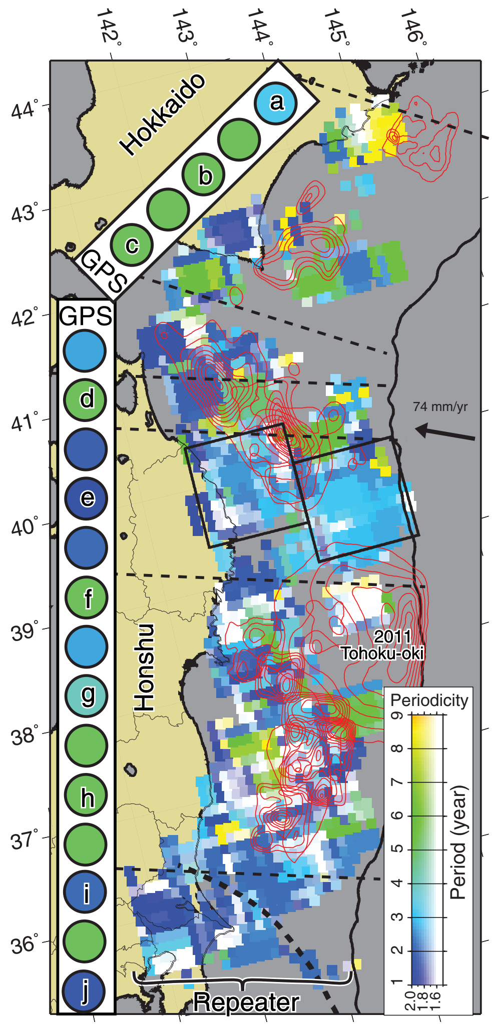

Fig. 4. Spatial distribution of degree of periodicity and dominant period estimated from the repeater data. The color intensity shows the degree of periodicity, and the colors show the dominant period for the periods from 1984 to 2011 (between 36.5° and 41.5°N) and from 1993 to 2011 (north of 41.5°N and south of 36.5°N). The periods indicated for each area represent the dominant peak in the amplitude spectrum of the slip-velocity variations inferred from repeaters for 0.4° (latitude) by 0.6° (longitude) spatial windows. Contours show slip areas for the 2011 Tohoku-oki earthquake (*M* 9.0) and other *M* 7 or larger earthquakes since 1930 (*11*–*13*, *30*). Colored circles show the dominant period of the on-land GPS gradient in plate motion parallel to the N105°E (Honshu) and N120°E (Hokkaido) directions (see fig. S13 for the spectrum of gradient time series in profile lines a to j that are used to compute the dominant periods).

REFERENCES AND NOTES

1. K. Heki, S. Miyazaki, H. Tsuji, *Nature* **386**, 595–598 (1997).
2. G. Dragert, K. Wang, T. S. James, *Science* **292**, 1525–1528 (2001).
3. P. Segall, A. M. Bradley, *Geophys. Res. Lett.* **39**, L18308 (2012).
4. A. Kato *et al.*, *Science* **335**, 705–708 (2012).
5. M. Bouchon, V. Durand, D. Marsan, H. Karabulut, J. Schmittbuhl, *Nat. Geosci.* **6**, 299–302 (2013).
6. S. Ruiz *et al.*, *Science* **345**, 1165–1169 (2014).
7. S. Ozawa, H. Suito, M. Tobita, *Earth Planets Space* **59**, 1241–1245 (2007).
8. R. M. Nadeau, T. V. McEvilly, *Science* **285**, 718–721 (1999).
9. R. M. Nadeau, T. V. McEvilly, *Science* **303**, 220–222 (2004).
10. N. Uchida, T. Matsuzawa, *Earth Planet. Sci. Lett.* **374**, 81–91 (2013).
11. Y. Yamanaka, M. Kikuchi, *Earth Planets Space* **55**, e21–e24 (2003).
12. Y. Yamanaka, M. Kikuchi, *J. Geophys. Res.* **109**, B07307 (2004).
13. T. Iinuma *et al.*, *J. Geophys. Res.* **117**, B07409 (2012).
14. Materials and methods are available as supplementary materials on *Science* Online.
15. G. F. Sella, T. H. Dixon, A. Mao, *J. Geophys. Res.* **107**, 2081 (2002).
16. N. Uchida, A. Hasegawa, T. Matsuzawa, T. Igarashi, *Tectonophysics* **385**, 1–15 (2004).
17. D. Marsan, T. Reverso, A. Helmstetter, B. Enescu, *J. Geophys. Res. Solid Earth* **118**, 4900–4909 (2013).
18. Y. Ito *et al.*, *Tectonophysics* **600**, 14–26 (2013).
19. T. J. Ader, J.-P. Avouac, *Earth Planet. Sci. Lett.* **377–378**, 97–105 (2013).
20. J. C. Savage, *J. Geophys. Res. Solid Earth* **88**, 4984–4996 (1983).
21. K. Heki, *Earth Planet. Sci. Lett.* **207**, 159–164 (2003).
22. Y. Tanaka, *Geophys. J. Int.* **196**, 760–787 (2014).
23. F. F. Pollitz, A. Wech, H. Kao, R. Bürgmann, *J. Geophys. Res. Solid Earth* **118**, 2445–2459 (2013).
24. Y. Liu, *Geophys. Res. Lett.* **40**, 1311–1316 (2013).
25. P. Segall, A. M. Rubin, A. M. Bradley, J. R. Rice, *J. Geophys. Res. Solid Earth* **115**, B12305 (2010).
26. P. Audet, R. Bürgmann, *Nature* **510**, 389–392 (2014).
27. R. Hino *et al.*, *Mar. Geophys. Res.* **35**, 181–190 (2014).
28. S. Ozawa *et al.*, *J. Geophys. Res.* **117**, B07404 (2012).
29. T. H. Jordan, L. M. Jones, *Seismol. Res. Lett.* **81**, 571–574 (2010).
30. T. Murotani, M. Kikuchi, Y. Yamanaka, "Rupture processes of large Fukushima-Oki earthquakes in 1938," paper S052-004, presented at the 2003 Japan Geoscience Union, Chiba, Japan, 2003.

ACKNOWLEDGMENTS

We thank Y. Yabe, T. Matsuzawa, W. Nakamura, R. C. Turner, S. Tanaka, C. W. Johnson, W. L. Ellsworth, Y. Ogata, and A. Hasegawa for fruitful discussion. The anonymous reviewers were helpful in greatly improving the manuscript. This work was supported in part by Japan Society for the Promotion of Science (JSPS) KAKENHI 23740328 and 15K05260 and the Ministry of Education, Culture, Sports, Science and Technology of Japan, under its Earthquake and Volcano Hazards Observation and Research Program. N.U. acknowledges support by Tohoku University under its Leading Young Researcher Overseas Visit Program. R.M.N. acknowledges support from the Berkeley Institute for Data Science, funded by the Moore-Sloan Data Science Environment Program. R.B. acknowledges support by U.S. NSF award EAR-1246850. R.H. acknowledges support by JSPS KAKENHI 26000002. The repeating earthquakes were selected based on the seismic waveforms from stations of Hokkaido University, Hirosaki University, Tohoku University, and the University of Tokyo. The repeating earthquake catalog is available as supplementary material on *Science* Online. The Japan Meteorological Agency (JMA) earthquake catalog used in this study is available at www.jma.go.jp, subject to the policies of the JMA. The GEONET F3 GPS solutions used in this study are available at www.gsi.go.jp, subject to the policies of the Geospatial Information Authority of Japan.

SUPPLEMENTARY MATERIALS

www.sciencemag.org/content/351/6272/488/suppl/DC1
Materials and Methods
Figs. S1 to S14
Tables S1 to S4
References (*31*–*42*)

26 August 2015; accepted 22 December 2015
10.1126/science.aad3108